Applied Physics Letters

Long-range ferromagnetic ordering in vanadium-doped WSe_2 semiconductor

Cite as: Appl. Phys. Lett. **115**, 242406 (2019); https://doi.org/10.1063/1.5131566
Submitted: 14 October 2019 . Accepted: 25 November 2019 . Published Online: 12 December 2019

Dinh Loc Duong, Seok Joon Yun, Youngkuk Kim, Seong-Gon Kim, and Young Hee Lee

Applied Physics Letters ARTICLE scitation.org/journal/apl

Long-range ferromagnetic ordering in vanadium-doped WSe_2 semiconductor

Cite as: Appl. Phys. Lett. **115**, 242406 (2019); doi: 10.1063/1.5131566
Submitted: 14 October 2019 · Accepted: 25 November 2019 ·
Published Online: 12 December 2019

Dinh Loc Duong,[1,2,a),b)] Seok Joon Yun,[1,2,a)] Youngkuk Kim,[1,3] Seong-Gon Kim,[4] and Young Hee Lee[1,2,3,b)]

AFFILIATIONS

[1]Center for Integrated Nanostructure Physics (CINAP), Institute for Basic Science (IBS), Suwon 16419, South Korea
[2]Department of Energy Science, Sungkyunkwan University, Suwon 16419, South Korea
[3]Department of Physics, Sungkyunkwan University, Suwon 16419, South Korea
[4]Department of Physics and Astronomy, Mississippi State University, Mississippi State, MS 39762, USA

[a)]**Contributions:** D. L. Duong and S. J. Yun contributed equally to this work.
[b)]**Electronic addresses:** ddloc@skku.edu and leeyoung@skku.edu

ABSTRACT

We report long-range ferromagnetic ordering in a vanadium-doped monolayer WSe_2 semiconductor using spin-polarized density functional calculations. We found that the vanadium dopant is located in the fully occupied state inside the valence band, inherent from spin–orbit coupling, leading to the presence of free holes in the valence band. As a consequence, the spin-polarized hole carriers are delocalized not only in the vanadium site but also persistently in the tungsten sites distant from vanadium to facilitate the long-range ferromagnetic ordering in the vanadium-doped monolayer WSe_2. Our findings of this study pave the way for the future exploration of carrier-mediated room-temperature two-dimensional ferromagnetic semiconductors via magnetic dopants.

A semiconductor in which a minute content of magnetic dopant is dissolved is called a dilute magnetic semiconductor (DMS). A DMS can create spin-polarized carriers, wherein the magnetic ordering is controlled by gating.[1–3] Although DMSs have been demonstrated in II-VI and III-V compounds such as Mn-doped CdTe and GaAs,[4–6] the stabilization of long-range ferromagnetic ordering is debatable, let alone the room temperature issue.[1–3,7–15] The primary concern is whether the magnetic order is established by the direct exchange between localized dopant states (e.g., impurity band model)[11–13] or the indirect exchange mediated by interaction with free carriers of host materials [e.g., Ruderman–Kittel–Kasuya–Yosida (RKKY) or the Zener model].[7,8,10,14,15] The difficulties originate from interstitial substitutions, clusters, and alloy formation, which give rise to completely different electronic band structures from the host materials.[8] The structure becomes even more complicated in oxides such as zinc and titanium oxides owing to their oxygen vacancies and nonstoichiometric structures.[16]

Semiconductors of the transition metal dichalcogenides (TMDs) are attractive hosts for DMSs; they may provide a unique opportunity to explore magnetic properties and improve the Curie temperature.[17–46] Recently, the room-temperature ferromagnetic ordering revealed by magnetic force microscopy at a low vanadium-doping concentration in WSe_2 has been observed.[31] Understanding the way long-range ferromagnetic ordering can be implemented plays an important role in achieving the gate-modulated magnetic properties of this material. The diluted magnetic TMD semiconductors have been previously investigated by density functional calculations.[17,20–27,29,30,32,34,36,37,40–46] However, how the long-range magnetic order is established with a low doping concentration has not been studied yet. It is also important to include the spin–orbit coupling (SOC) in TMDs to investigate their magnetic properties, in particular for the V-doped WSe_2 system to understand the possibility of long-range spin order formation. Here, the band structure of V-doped WSe_2 is investigated by spin-polarized density functional calculations with 8×8 and 10×10 supercells that correspond to 1.6% and 1% of vanadium. We found that spin–orbit coupling (SOC) plays a key role in provoking the long-range ferromagnetic order in V and W sites far away from V positions through the free hole carriers. This supports the RKKY model.

The band structure was calculated by density functional theory (DFT) using the Quantum Espresso package with generalized gradient approximation (GGA) plus U ($U = 3$).[47,48] The projector augmented wave pseudopotentials were used with a cutoff energy of 80 Ry.[49] The structure was optimized with a force smaller than 0.05 eV·Å^{-1} and an

energy convergence of 0.02 meV/atom. The energy convergence threshold for each self-consistence step is 10^{-6} eV. To isolate the interaction between the layers, a length of 20 Å along the c-axis was used. As the 8×8 and 10×10 supercells contain a large number of atoms, a cutoff energy of 30 Ry with the Gamma point was used for the self-consistent calculation. The lattice constant of the optimized WSe_2 was used to calculate the doped structure. There was a negligible change in the pressure of the supercell, which indicates a small change in the structure of the V-doped WSe_2. In both the calculations (with and without SOC), the magnetic moment is initially introduced along the z-axis (parallel to the *c*-axis). To check the cutoff energy convergence, the 6×6 supercell with a 4×4 k-grid was used. The band orders with cutoff energies of 30 and 80 Ry are similar (Fig. S1). Therefore, using the 30 Ry cutoff energy result is not detrimental to our conclusions. The trend observed in our results is the same as that calculated in the cases of MoS_2 and WSe_2 using local density approximation (LDA), generalized gradient approximation (GGA), and GGA+U functionals.[35]

Figure 1(a) depicts the band structure of the 8×8 supercell of the V-doped WSe_2 monolayer obtained from the DFT-GGA+U calculations without SOC. U is chosen as 3 to describe the strong Coulomb interaction of vanadium.[50,51] The Fermi level of the V-doped WSe_2 is shifted down near the valence band, thereby exhibiting the p-doping effect with the V dopant compared to the Fermi level located in the center of the bandgap (Fig. S2). A localized spin-down state, which is unoccupied and shallow near the band edge (approximately 0.05 eV above the Fermi level), is ascribed to an acceptor in the p-doped WSe_2. The difference between the spin-up and the (dominant) spin-down state clearly indicates the spin-polarized band structure of the V-doped WSe_2 and, in particular, the spin-polarized top valence band. We note that the maximum valence band in the WSe_2 monolayer is located at the K_1 point of the primitive cell.[52] Although the band folding occurs in the 8×8 unit cell, the K points of the primitive (K_1) and the 8×8 supercell (K_8) are coincident, which gives rise to the maximum of the valence band located at the K_8 point of the 8×8 unit cell (Fig. S3).

The strong SOC of the W atom splits the valence band edge of WSe_2.[53] This band splitting can strongly influence the characteristics of the V-dopant. Therefore, it is important to examine the effect of SOC on the band structure of the V-doped WSe_2. With SOC, the Fermi level shifts down inside the valence band edge [Fig. 1(b)], which is distinct from the Fermi level located above the valence band edge. The spin energy difference between the ferromagnetic and nonmagnetic states is 340 meV, which is much higher than 140 meV without SOC. The Curie temperature is 2600 K by rough estimation using mean field theory,[54] i.e., $T_c = 2\Delta_E/3k_B$. This result of mean field theory is usually overestimated. With SOC, the total spin magnetic moment with a particular V-doping concentration of 1.6% is enhanced by 40%. The long-range order of the spin system is clearly manifested with SOC and has not been found to be discernable without SOC. This is described in the subsequent sections. We note that the top of valence bands of the pristine and doped structures is overleaped, indicating the similar effective mass of these two bands (Fig. S4). Therefore, degradation of mobility owing to the change in the effective mass is negligible. Nevertheless, the doping state generated by the strong hybridization of V, W, and Se atoms can be a scattering center, which reduces the mobility of pristine WSe_2. It is unavoidable in the doped systems.

To investigate the contribution of the V and W atoms to the band structure, their projected density of states (PDOS) is provided in Fig. 2(a).

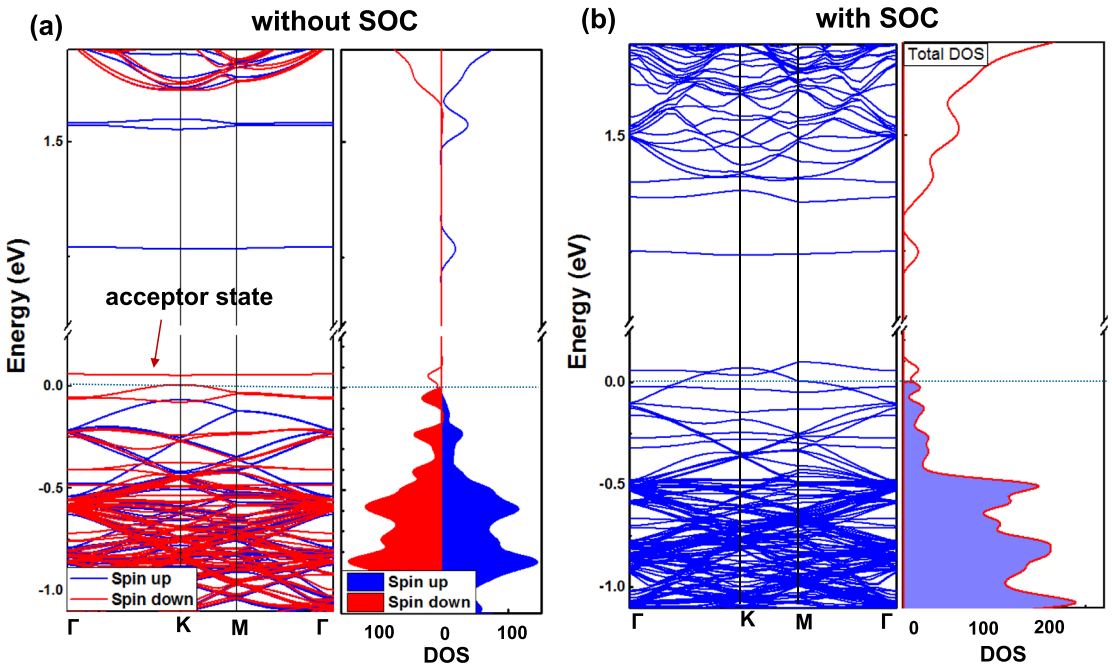

FIG. 1. Spin-polarized band structure and total DOSs of V-doped WSe_2 (a) without SOC and (b) with SOC of the 8×8 supercell. The blue and red colors represent the corresponding spin-up and spin-down density of states in the case of no SOC.

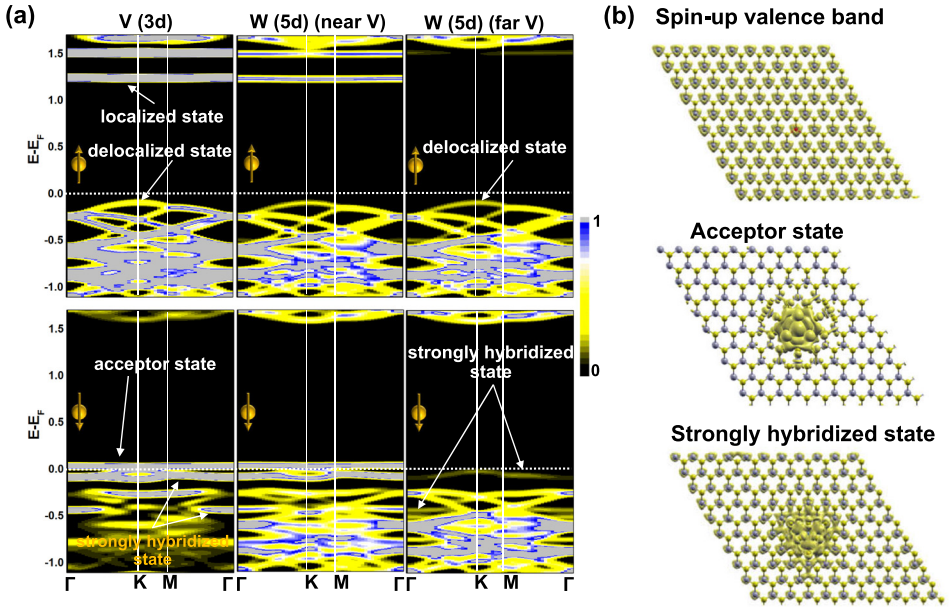

FIG. 2. (a) Partial d-orbital density of states of V-doped WSe_2 at the V atom and the W atoms near the V and far from the V sites. The color mapping represents the density of states at different k-points from 0 to 1 state/eV. (b) Spatial distribution of density of states near the Fermi level. The values of isosurfaces are 0.000 025, 0.0001, and 0.000 05 states/(Bohr^3 Ry) for the corresponding spin-up valence band, acceptor, and strongly hybridized states.

The V-dopant-related spin structures without SOC are visualized more intuitively than those with SOC even though the overall band structures are similar to each other except for the location of the Fermi level close to the valence band edge (Fig. S5). Several states of the projected V atom are distinct: (i) flat dispersion in both spin-up near conduction bands and spin-down near valence bands, (ii) delocalized bands, and (iii) strongly hybridized bands. The spin-up and one spin-down states are localized as a flatband from the V site corresponding to near conduction and valence band edges.

While the V delocalized states contribute to the whole energy range of the valence band, strong hybridization between the d-orbitals of the V and W sites (left and middle panels) is clearly visualized in the projected DOSs. The localized d-orbitals of the W atom near the V site are similar to those of the V site. In contrast, the localized d-orbitals disappear at the W site far away from the V site. Moreover, the p-orbital of Se atoms near the V site is also revealed at the localized doping level, thereby indicating the pd-d interaction between the V, W, and Se atoms of these localized states. Intriguingly, the spin-polarized states are still persistent even at the W site far away from the V site (right panel). The strong hybridization between the V and W atoms takes place at all the W sites even far away from the V site (bottom of the right panel).

Next, the partial local density of states in real space is calculated to elucidate the delocalization degree of the doping states. The spin-up state is uniformly distributed over the entire W atoms including the V site by the significant contribution in the valence band edge (top panel) [Fig. 2(b)]. In contrast, the spin-down acceptor state near the Fermi level (middle panel) is strongly localized near the V site, extending over two- or three-unit cells of WSe_2. The strongly hybridized states are also delocalized with high density of states near the V site, slowly decaying far from the V site. It is observed that the DOS of the Se atoms far from the V site is negligible for the strong hybridization state (Fig. S6). This implies the nature of the d-d interaction solely between the V and W atoms of this state. Similar types of bands are also observed with SOC, except the number of bands, which is larger than that without SOC due to band splitting (Fig. S5).

Next, the long-range magnetic order in V-doped WSe_2 is verified. As the free carriers of the host materials manifest the long-range magnetic ordering, the local magnetic moment in real space is calculated. The projection of the spin density along the c axis for the same color scale of 0.0007 $\mu_B/Å^2$ was investigated with and without SOC (Fig. 3). The magnetic moment is highly localized near the V sites without SOC [Fig. 3(a)]. The magnetic moment on the W atoms far from the V atom (Table I) is negligible. In contrast, the spin density with SOC expands to the entire W atoms even far from the V atom [Figs. 3(b), S7, and Table I]. This clearly demonstrates the long-range magnetic order. The contribution of the spin density far from the Se atoms is negligible. The W atoms far from the V atom have spin-up electrons similar to the spin state of the V atom, whereas other W atoms nearest to the V atom contain spin-down electrons (Table I). The magnetic moment is enhanced by the average of the entire lattice. Further, the magnetic moment for the 10×10 unit cell corresponding to 1% V concentration with a V–V distance of 3.5 nm is calculated (Figs. S8 and S9). The long-range spin order is also similar in the case of the

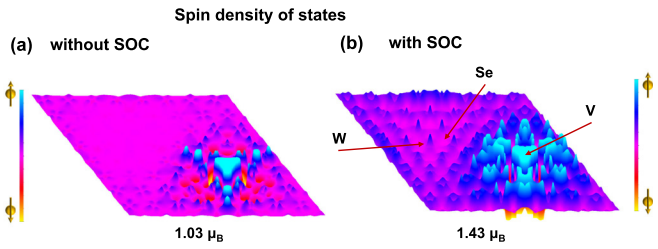

FIG. 3. Projected magnetic moments along the c axis (*a*) without SOC and (*b*) with SOC of the 10×10 supercell. The color map range is from -0.0007 to 0.0007 $\mu_B/Å^2$ for the spin-down and spin-up states.

TABLE I. Spin density of W atoms with their distance from the V site in the 10 × 10 supercell.

		V	W1	W2	W3	W4	W5
Distance from V site (Å)		0	3.28	6.55	9.83	13.11	16.39
Magnetic moments (μ_B)	no-SOC	1.0310	−0.0055	0.0018	0.0005	0.0002	0.0002
	SOC	1.0546	−0.0189	0.0068	0.0037	0.0021	0.0017

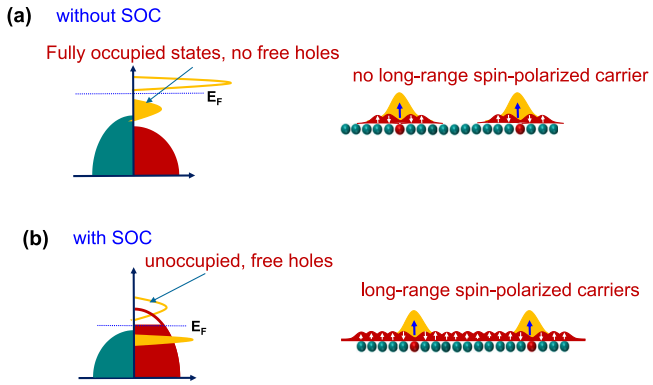

FIG. 4. Schematic band structure of V-doped WSe_2 (a) without SOC and (b) with SOC for the corresponding magnetic moments distributed in real space.

8 × 8 unit cell. It is worth mentioning that the well-known issue of the bandgap underestimation by GGA and GGA+U can give rise to erroneous positions of the doping level.[55] However, it is confirmed that the GGA+U scheme produces doping levels comparable to Heyd-Scuseria-Ernzerhof calculations,[35] which are widely expected to result in a bandgap closer to the experimental value. Therefore, these results with GGA+U are still valid.

The simple band model of the V-doped WSe_2 with and without SOC is summarized in Fig. 4. Without SOC, the strongly hybridized states are fully occupied near the valence band edge below the Fermi level. No free holes are available in the valence band edge. Therefore, the magnetic moments are induced locally near the V site with a minor contribution of the spin-down states [Fig. 4(a)]. Meanwhile, with SOC, the localized V band is inverted into the valence band edge, thereby leaving the spin-polarized hole carriers in the valence band [Fig. 4(b)]. Consequently, the long-range ferromagnetic order is mediated with free holes to establish the spin order even near the W sites in the entire lattice.

In conclusion, the long-range ferromagnetic order has been demonstrated in the V-doped WSe_2 monolayer. The SOC plays an important role in determining the energy level of the doping states, leading to the formation of spin-polarized free holes. The short-range *pd-d* hybridization among the V, W, and Se atoms and, more importantly, the long-range *d-d* hybridization solely between the V and W atoms are identified. The latter could play an important role in improving the Curie temperature in V-doped WSe_2.

See the supplementary material for the band structure of pristine WSe_2, PDOS analysis including SOC, and spin density of the 8 × 8 and 10 × 10 supercells.

This study was supported by the Institute for Basic Science of Korea (No. IBS-R011-D1). Y.K. gratefully acknowledges the support received from the National Research Foundation of Korea (NRF) in the form of the grant funded by the Korean government (MSIP; Ministry of Science, ICT and Future Planning) (No. 2019R1F1A1055205). The computational support was provided by the Korea Institute of Science and Technology Information (KISTI) under Grant Nos. KSC-2016-C3-0042 and KSC-2017-C2-0056.

REFERENCES

[1]T. Jungwirth, J. Sinova, J. Mašek, J. Kučera, and A. H. MacDonald, Rev. Mod. Phys. **78**, 809 (2006).
[2]K. Sato, L. Bergqvist, J. Kudrnovský, P. H. Dederichs, O. Eriksson, I. Turek, B. Sanyal, G. Bouzerar, H. Katayama-Yoshida, V. A. Dinh, T. Fukushima, H. Kizaki, and R. Zeller, Rev. Mod. Phys. **82**, 1633 (2010).
[3]T. Dietl and H. Ohno, Rev. Mod. Phys. **86**, 187 (2014).
[4]H. Ohno, D. Chiba, F. Matsukura, T. Omiya, E. Abe, T. Dietl, Y. Ohno, and K. Ohtani, Nature **408**, 944 (2000).
[5]D. Chiba, H. Yamanouchi, F. Hatsukura, and H. Ohno, Science **301**, 943 (2003).
[6]M. Yamanouchi, D. Chiba, F. Matsukura, and H. Ohno, Nature **428**, 539 (2004).
[7]T. Dietl, Semicond. Sci. Technol. **17**, 377 (2002).
[8]T. Dietl, Nat. Mater. **9**, 965 (2010).
[9]A. H. Macdonald, P. Schiffer, and N. Samarth, Nat. Mater. **4**, 195 (2005).
[10]A. Bonanni and T. Dietl, Chem. Soc. Rev. **39**, 528 (2010).
[11]S. Ohya, K. Takata, and M. Tanaka, Nat. Phys. **7**, 342 (2011).
[12]M. Dobrowolska, K. Tivakornsasithorn, X. Liu, J. K. Furdyna, M. Berciu, K. M. Yu, and W. Walukiewicz, Nat. Mater. **11**, 444 (2012).
[13]N. Samarth, Nat. Mater. **11**, 360 (2012).
[14]S. Souma, L. Chen, R. Oszwałdowski, T. Sato, F. Matsukura, T. Dietl, H. Ohno, and T. Takahashi, Sci. Rep. **6**, 27266 (2016).
[15]T. Dietl, H. Ohno, F. Matsukura, J. Cibert, and D. Ferrand, Science **287**, 1019 (2000).
[16]S. B. Ogale, "Dilute Doping, Defects, and Ferromagnetism in Metal Oxide Systems," Adv. Mater. **22**, 3125 (2010).
[17]C. Ataca and S. Ciraci, J. Phys. Chem. C **115**, 13303 (2011).
[18]K. Dolui, I. Rungger, C. Das Pemmaraju, and S. Sanvito, Phys. Rev. B **88**, 075420 (2013).
[19]Y. C. Lin, D. O. Dumcenco, H. P. Komsa, Y. Niimi, A. V. Krasheninnikov, Y. S. Huang, and K. Suenaga, Adv. Mater. **26**, 2857 (2014).
[20]C. J. Gil, A. Pham, A. Yu, and S. Li, J. Phys.: Condens. Matter **26**, 306004 (2014).
[21]Y. Miao, Y. Huang, Q. Fang, Z. Yang, K. Xu, F. Ma, and P. K. Chu, J. Mater. Sci. **51**, 9514 (2016).
[22]X. Zhao, C. Xia, T. Wang, and X. Dai, J. Alloys Compd. **654**, 574 (2016).
[23]A. W. Robertson, Y. C. Lin, S. Wang, H. Sawada, C. S. Allen, Q. Chen, S. Lee, G. Do Lee, J. Lee, S. Han, E. Yoon, A. I. Kirkland, H. Kim, K. Suenaga, and J. H. Warner, ACS Nano **10**, 10227 (2016).
[24]N. Singh and U. Schwingenschlögl, ACS Appl. Mater. Interfaces **8**, 23886 (2016).
[25]Y. Wang, S. Li, and J. Yi, Sci. Rep. **6**, 24153 (2016).

[26]M. Luo, Y. H. Shen, and J. H. Chu, Jpn. J. Appl. Phys., Part 1 **55**, 093001 (2016).
[27]N. Singh and U. Schwingenschlögl, Adv. Mater. **29**, 1600970 (2017).
[28]V. Kochat, A. Apte, J. A. Hachtel, H. Kumazoe, A. Krishnamoorthy, S. Susarla, J. C. Idrobo, F. Shimojo, P. Vashishta, R. Kalia, A. Nakano, C. S. Tiwary, and P. M. Ajayan, Adv. Mater. **29**, 1703754 (2017).
[29]Q. Yue, S. Chang, S. Qin, and J. Li, Phys. Lett. A **377**, 1362 (2013).
[30]C. H. Ho, W. H. Chen, K. K. Tiong, K. Y. Lee, A. Gloter, A. Zobelli, O. Stephan, and L. H. G. Tizei, ACS Nano **11**, 11162 (2017).
[31]S. J. Yun, D. L. Duong, M.-H. Doan, K. Singh, T. L. Phan, W. Choi, Y.-M. Kim, and Y. H. Lee, "Room-temperature ferromagnetism in monolayer WSe2 semiconductor via vanadium dopant," e-print arXiv:1806.06479.
[32]Y. Miao, Y. Li, Q. Fang, Y. Huang, Y. Sun, K. Xu, F. Ma, and P. K. Chu, Appl. Surf. Sci. **428**, 226 (2018).
[33]M. Habib, Z. Muhammad, R. Khan, C. Wu, Z. ur Rehman, Y. Zhou, H. Liu, and L. Song, Nanotechnology **29**, 115701 (2018).
[34]B. Xia, P. Liu, Y. Liu, D. Gao, D. Xue, and J. Ding, Appl. Phys. Lett. **113**, 013101 (2018).
[35]M. Wu, X. Yao, Y. Hao, H. Dong, Y. Cheng, H. Liu, F. Lu, W. Wang, K. Cho, and W. H. Wang, Phys. Lett. A **382**, 111 (2018).
[36]P. M. Coelho, H. Komsa, K. Lasek, V. Kalappattil, J. Karthikeyan, M. Phan, A. V. Krasheninnikov, and M. Batzill, Adv. Electron. Mater. **5**, 1900044 (2019).
[37]Y. Gao, N. Ganguli, and P. J. Kelly, Phys. Rev. B **99**, 220406 (2019).
[38]S. Ahmed, X. Ding, P. P. Murmu, N. Bao, R. Liu, J. Kennedy, L. Wang, J. Ding, T. Wu, A. Vinu, and J. Yi, "High coercivity and magnetization in WSe_2 by codoping Co and Nb," Small (published online).
[39]K. Zhang, S. Feng, J. Wang, A. Azcatl, N. Lu, R. Addou, N. Wang, C. Zhou, J. Lerach, V. Bojan, M. J. Kim, L. Q. Chen, R. M. Wallace, M. Terrones, J. Zhu, and J. A. Robinson, Nano Lett. **15**, 6586 (2015).
[40]R. Mishra, W. Zhou, S. J. Pennycook, S. T. Pantelides, and J.-C. Idrobo, Phys. Rev. B **88**, 144409 (2013).
[41]A. Ramasubramaniam and D. Naveh, Phys. Rev. B **87**, 195201 (2013).
[42]Y. C. Cheng, Z. Y. Zhu, W. B. Mi, Z. B. Guo, and U. Schwingenschlögl, Phys. Rev. B **87**, 100401 (2013).
[43]A. N. Andriotis and M. Menon, Phys. Rev. B **90**, 125304 (2014).
[44]W. S. Yun and J. D. Lee, Phys. Chem. Chem. Phys. **16**, 8990 (2014).
[45]J. Qi, X. Li, X. Chen, and K. Hu, J. Phys.: Condens. Matter **26**, 256003 (2014).
[46]S.-C. Lu and J.-P. Leburton, Nanoscale Res. Lett. **9**, 676 (2014).
[47]P. Giannozzi, S. Baroni, N. Bonini, M. Calandra, R. Car, C. Cavazzoni, D. Ceresoli, G. L. Chiarotti, M. Cococcioni, I. Dabo, A. Dal Corso, S. de Gironcoli, S. Fabris, G. Fratesi, R. Gebauer, U. Gerstmann, C. Gougoussis, A. Kokalj, M. Lazzeri, L. Martin-Samos, N. Marzari, F. Mauri, R. Mazzarello, S. Paolini, A. Pasquarello, L. Paulatto, C. Sbraccia, S. Scandolo, G. Sclauzero, A. P. Seitsonen, A. Smogunov, P. Umari, and R. M. Wentzcovitch, J. Phys.: Condens. Matter **21**, 395502 (2009).
[48]P. Giannozzi, O. Andreussi, T. Brumme, O. Bunau, M. Buongiorno Nardelli, M. Calandra, R. Car, C. Cavazzoni, D. Ceresoli, M. Cococcioni, N. Colonna, I. Carnimeo, A. Dal Corso, S. de Gironcoli, P. Delugas, R. A. DiStasio, A. Ferretti, A. Floris, G. Fratesi, G. Fugallo, R. Gebauer, U. Gerstmann, F. Giustino, T. Gorni, J. Jia, M. Kawamura, H.-Y. Ko, A. Kokalj, E. Küçükbenli, M. Lazzeri, M. Marsili, N. Marzari, F. Mauri, N. L. Nguyen, H.-V. Nguyen, A. Otero-de-la-Roza, L. Paulatto, S. Poncé, D. Rocca, R. Sabatini, B. Santra, M. Schlipf, A. P. Seitsonen, A. Smogunov, I. Timrov, T. Thonhauser, P. Umari, N. Vast, X. Wu, and S. Baroni, J. Phys.: Condens. Matter **29**, 465901 (2017).
[49]E. Kucukbenli, M. Monni, B. I. Adetunji, X. Ge, G. A. Adebayo, N. Marzari, S. de Gironcoli, and A. D. Corso, "Projector augmented-wave and all-electron calculations across the periodic table: a comparison of structural and energetic properties," e-print arXiv:1404.3015.
[50]L. Wang, T. Maxisch, and G. Ceder, Phys. Rev. B **73**, 195107 (2006).
[51]M. Kan, B. Wang, Y. H. Lee, and Q. Sun, Nano Res. **8**, 1348 (2015).
[52]I. Tanabe, T. Komesu, D. Le, T. B. Rawal, E. F. Schwier, M. Zheng, Y. Kojima, H. Iwasawa, K. Shimada, T. S. Rahman, and P. A. Dowben, J. Phys.: Condens. Matter **28**, 345503 (2016).
[53]L. Le, D. Barinov, A. Preciado, E. Isarraraz, M. Tanabe, I. Komesu, T. Troha, and C. Bartels, J. Phys.: Condens. Matter **27**, 182201 (2015).
[54]N. Seña, A. Dussan, F. Mesa, E. Castaño, and R. González-Hernández, J. Appl. Phys. **120**, 051704 (2016).
[55]L. Blinov, A. Bune, P. Dawben, S. Ducharme, V. Fridkin, S. Palto, K. Verkhovskaya, G. Vizdrik, and S. Yudin, Phase Transitions **77**, 161 (2004).